Revue des Composites et des Matériaux Avancés-Journal of Composite and Advanced Materials
Vol. 34, No. 2, April, 2024, pp. 177-188
Journal homepage: http://iieta.org/journals/rcma

An Analytical Analysis of the Hydrostatic Bending to Design a Wastewater Treatment Plant by a New Advanced Composite Material

Abdeldjalil Benbakhti[1*], Abdelmoutalib Benfrid[2], Zouaoui R. Harrat[2], Mohammed Chatbi[2], Mohammed Bachir Bouiadjra[2,3], Baghdad Krour[2]

[1] Department of Hydraulics and Civil Engineering-Institute of Technology, Maghnia University Centre, Maghnia 13000, Algeria
[2] Laboratoire des Structures et Matériaux Avancés dans le Génie Civil et Travaux Publics, University of Djillali Liabes, Sidi Bel-Abbes 22000, Algeria
[3] Thematic Agency for Research in Science and Technology, ATRST, Algiers 16000, Algeria

Corresponding Author Email: Jalil7benbakhti@gmail.com

https://doi.org/10.18280/rcma.340207

Received: 22 December 2023
Revised: 15 April 2024
Accepted: 21 April 2024
Available online: 29 April 2024

Keywords:
advanced composite material, bending analysis, wastewater treatment plant, analytical analysis, hydrostatic loads

ABSTRACT

In recent years, many countries have been confronted with an extended period of drought, necessitating innovative water supply solutions for both human consumption and agricultural irrigation. In response, wastewater treatment plants (WWTPs) have emerged as pivotal agents in water recycling, catering to agricultural needs and environmental considerations. These plants facilitate the transformation of wastewater into potable or irrigation-ready water. Amidst the array of WWTP designs, the "Continuous-Station" holds a distinctive position, featuring a monolithic steel-structure meticulously crafted from either conventional or stainless-steel. Presently, the prevalent approach involves the application of anti-corrosion paint to protect this monolithic structure from the corrosive effects of aggressive substances present in wastewater. However, an innovative strategy is being explored – the incorporation of tungsten, an anti-corrosive element, into the stainless-steel alloy. This integration shows promising potential to enhance resilience against the relentless degradation forces within wastewater, simultaneously bolstering the mechanical properties of the steel. This research paper exclusively focuses on analyzing, analytically, the hydrostatic bending performance of WWTP structural components infused with nano-tungsten-particles. The range of incorporation spans from a baseline of 0%, representing the steel without any infusion, to an optimal threshold of 30% relative to the overall volume of the steel matrix. The elastic-properties of the composite steel-tungsten alloy are characterized using Mori-Tanaka's homogenization model. The WWPT structural components are simplified as plates and analyzed using an advanced mathematical model based on the refined plate theory. The outcomes underscore a notable enhancement in flexural strength by augmenting the fraction of tungsten nanoparticles within the stainless-steel matrix.

1. INTRODUCTION

Climate change has taken a prominent toll on Algeria in recent times, culminating in severe drought conditions, particularly accentuated in the last decade. This alarming issue has significantly impacted the nation's agricultural sector [1]. The ramifications of climate change are manifest through escalated air temperatures, the melting of glaciers, rising sea levels, aggravated desertification, and a surge in extreme weather events encompassing heat waves, droughts, floods, and storms. Notably, the impact of climate change varies across regions, imposing disproportionate effects on different areas [2]. To elucidate the transformations observed within the Algerian locale spanning the last forty years, we present in Figure 1 a graphical depiction that relies on ERA5 data, sourced from the fifth-generation ECMWF Atmospheric Analysis of Global Climate. Encompassing the temporal span from 1979 to 2021 and boasting a spatial resolution of 30 km, this dataset furnishes a holistic vantage point pertaining to the dynamic evolution of the climatic milieu [3].

The profound ramifications of this climate-induced metamorphosis have triggered a surge in comprehensive investigations, seeking to unravel its multifaceted effects on Algerian agricultural practices. The in-depth econometric analysis covering the years 1980 to 2020, entitled "Impact of Climate Change on Agricultural Production in Algeria", represents a major scientific effort in this field. This study, aspired to proffer a comprehensive assessment of the intricate repercussions within Algerian agriculture, notably directs attention to the preceding two decades a span during which a staggering 30% reduction in precipitation levels has unfurled across the nation, in turn precipitating a consequential and

disquieting decline in agricultural productivity [4].

Compelling statistics furnished by Algeria's national bureau serve to underscore the gravity of this situation, portraying a disconcerting 30% downturn in agricultural yield within the western region. More alarmingly, the eastern region bears witness to a pronounced 40% decrement over this same pivotal time frame [5, 6], as visually elucidated in Figure 2. This distressing trajectory places the agricultural sector on a precipitous course, grappling with the dual challenges of diminishing rainfall and localized production.

The confluence of these challenges has galvanized the need for effective and expedient remedial measures. In response, the Ministry of Hydraulics has taken resolute steps, adopting a strategic policy that pivots around the innovative reuse of wastewater. The trajectory of this wastewater treatment initiative is artfully delineated in Figure 3, embodying the overarching aim of establishing wastewater treatment protocols that synergistically dovetail with sustainable agricultural practices [7].

In the context of wastewater treatment, a wide variety of approaches come into play, encompassing diverse methods such as biological treatment utilizing activated sludge, treatment through trickling filters, lagooning, membrane filtration, and UV disinfection [8]. These methods can be implemented using an array of materials, ranging from steel, reinforced concrete, and PVC, to cut stones and compact backfilled substances. Among the numerous designs for wastewater treatment plants, one notable innovation takes the form of the "Continuous Station," distinguished by its monolithic structure. While upholding the foundational principles of conventional treatment plants, this design stands out by virtue of its compact footprint, providing an efficient solution tailored to environments with spatial limitations.

As illustrated in Figure 4, the operational rhythm of the monobloc station unveils a process underpinned by several key zones [9]:

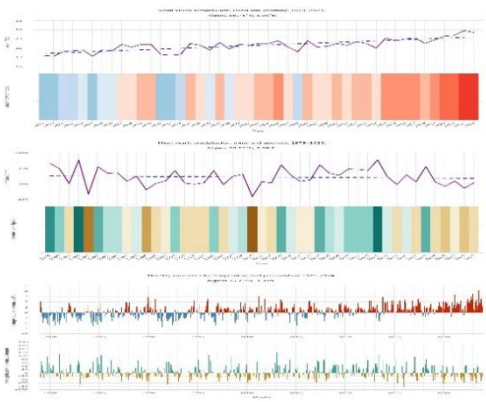

Figure 1. Precipitation and temperature change (Climate change in Algeria 1979-2021)

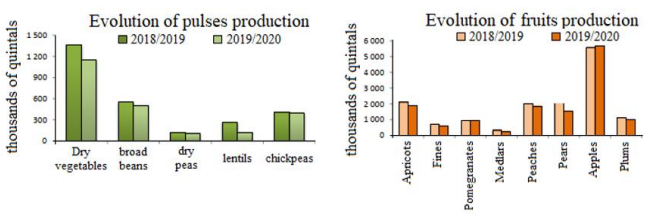

Figure 2. Statistics of the production of agricultural products in Algeria (2018-2020)

Figure 3. The water system in Algeria (drinkingwater-wasre water) with purification cycle

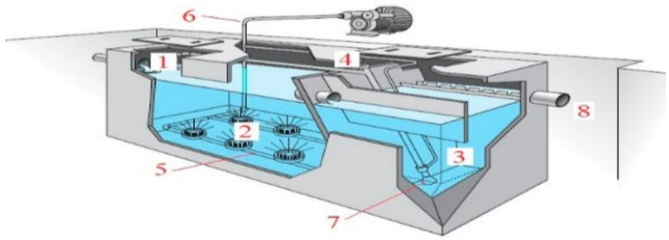

Figure 4. The system of purification by the contumely station or monobloc system

(1): An unventilated area housing a vertical flow labyrinth.
(2): A ventilated zone.
(3): A sedimentation zone.
(4): An integrated retention space.
(5): Internal recirculation.
(6): Recirculation of impurities.
(7): Aeration through the introduction of fine bubbles.
(8): Implementation of a flow regulator.

This specific design has found practical realization within Algeria, notably gaining prominence within the 'BABA-ALI' region nestled within the Wilaya of AIN DEFLA. Initially, this installation was executed using conventional steel, a choice that, while structurally robust, exposes the framework to potential corrosion due to the chemical constituents present in wastewater. Faced with this acknowledged vulnerability, our research endeavors to both address and circumvent these risks through the advocacy of an alternative material strategy—namely, the integration of a steel alloy fortified with tungsten nanoparticles.

The burgeoning field of nanotechnology has led to revolutionary advances in a number of sectors, construction engineering being no exception [10]. Nanoparticles, owing to their exceptional properties at the nanoscale, have ignited immense interest in their potential applications to enhance conventional construction materials [11]. These nanoparticles, including silicon oxide [12, 13], ferric oxide [14], alumina oxide [15], zircon [16], and titanium oxide [17], may have inherent limitations, but their potential can be unlocked through the strategic integration of nanoparticles. Nanoparticles exhibit unique behaviors due to their high surface area-to-volume ratio and quantum effects, making them versatile candidates for enhancing thermal, electrical, chemical, and mechanical properties of construction materials [18]. In civil engineering, nanoparticles have been extensively explored to bolster the performance of foundational materials like concrete and steel. This avenue of research has led to the development of materials with enhanced strength, durability, and multifunctionality [19].

In the context of thermal enhancement, nanoparticles have demonstrated remarkable potential by improving the thermal

conductivity of materials. This attribute is crucial for maintaining energy efficiency in construction, thereby contributing to sustainable infrastructure. For instance, Harrat et al. [20], investigated the thermoelastic bending behavior of concrete infused with ferric oxide nanoparticles. Similarly, Benfrid et al. [21], conducted an analytical study exploring the impact of glass powder additives on concrete beams exposed to thermal loading. Both studies concluded that the addition of these entities enhances the mechanical properties of concrete while concurrently affecting its thermal characteristics due to the nanoparticles' high thermal conductivity. In a separate study, Chatbi et al. [22] conducted a mechanical analysis of polymer structures reinforced with either aligned or randomly aligned carbon nanotubes using the MORI-TANAKA approach. The findings highlighted a significant enhancement in the mechanical properties of polymers due to carbon nanotubes reinforcement. The same authors also performed an analytical investigation on the mechanical response of concrete beams reinforced with various types of clay nanoparticles, emphasizing the enhancement capabilities of these additives through a strategic integration [23]. Still in the realm of construction materials, nanocomposites offer the promise of greater strength, enhanced ductility, improved and corrosion resistance. For example, research by Long et al. [24] has shown that the addition of nano-sized reinforcements, such as graphene oxide nanosheets, can significantly increase the dynamic mechanical properties of cement paste. Similarly, studies by Behzadian and Shahrajabian [25], Wang et al. [26], Zhang et al. [27] and Bhatta et al. [28] have explored the effects of incorporating silica nanoparticles on the mechanical and durability properties of cementitious materials, showing improvements in both strength and resistance to environmental degradation.

Additionally, nanoparticles have proven invaluable in electrically conductive composites, opening avenues for smart structures and sensors that can monitor and adapt to changing environmental conditions. McCall [29] and Magnani et al. [30], have discussed the piezoelectric properties of nano-infused polymers. Furthermore, new synthesis and characterization techniques have been developed as a result of recent advances in nanotechnology, giving researchers more precise control over the characteristics of nanocomposites. To improve dispersion and interfacial bonding, for instance, functionalized nanoparticles can be used to increase their compatibility with the matrix material [31-33].

The focus of this study centers on tungsten nanoparticles, a particular class of nanoparticles that hold promise as a formidable agent against corrosion in construction materials [34]. Corrosion poses a significant challenge in civil engineering, often resulting in deterioration and reduced lifespan of structures [35]. Tungsten, renowned for its exceptional anti-corrosion properties, has been investigated for its potential to mitigate the corrosive effects of harsh environments on construction materials. Burkov and Chigrin [36], performed an experimental study on the effect of tungsten, molybdenum, nickel and cobalt on the corrosion and wear performance of Fe-based metallic glass coatings. They concluded that doping metallic glass coatings with tungsten and nickel improves anticorrosion properties in both high-temperature oxidation and electrochemical corrosion.

Several other studies have confirmed the protective effect of tungsten against corrosion, for instant, Nishimura et al. [37] investigated the corrosion behavior of tungsten-bearing steel in a wet/dry environment containing chloride ions. This investigation aimed to address the challenges posed by force shortage, necessitating the use of weathering steels for minimal maintenance. Their findings indicated that utilizing tungsten coating and surface treatment in coastal areas had a beneficial effect on corrosion resistance. Liu et al. [38] explored the effects of a tungsten pre-implanted layer on the corrosion and electrochemical characteristics of amorphous carbon films on stainless steel. Their experimental findings demonstrated that the pre-implemented tungsten coating layer enhances the corrosion resistance of steel. Additionally, Xavier [39] delved into the impact of superior surface protection, mechanical strength, and hydrophobic properties of salinized tungsten carbide nanoparticles encapsulated within epoxy nanocomposite coatings on steel structures in marine environments. The results highlighted that the newly developed mercapto-propyltrimethoxysilane (MPTMS)/WC nanoparticles within the neat epoxy (EP) coated mild steel nanocomposite exhibited superior corrosion protection and enhanced hydrophobic behaviors (with a water contact angle of 144°). Furthermore, the investigated coatings displayed significant improvements in mechanical properties. Consequently, the compatibility of EP, MPTMS, and WC nanoparticles was established through their superior hydrophobicity, improved corrosion protection, and enhanced mechanical properties

Furthermore, beyond its anti-corrosion prowess, tungsten nanoparticles exhibit a dual role by reinforcing the mechanical integrity of materials [40]. The incorporation of these nanoparticles into steel alloys has demonstrated the capacity to enhance strength, ductility, and overall structural performance [41]. Increased tungsten particle content in tungsten-chromium metal matrix composite coatings increases wear resistance, according to Bartkowski et al. [42]. Such attributes are paramount in environments where construction materials are subjected to substantial loads, pressures, and potentially corrosive elements. Dong et al. [43], suggested the addition of tungsten carbide to enhance the mechanical properties of a graphene/copper matrix, replacing the low-dimensional nano-carbon materials as the interfaces between the nano-carbon materials and the metal matrix always present a significant challenge for achieving the best enhancement effects. They concluded that the addition of small amounts of tungsten can lead to a significant improvement in the tensile strength of the metal composite matrix. Research by Zhang et al. [44] investigated the use of tungsten fibers as reinforcement in polymer composites, highlighting their superior stiffness, strength, and thermal stability compared to conventional fibers such as glass or carbon. Moreover, studies by Liu et al. [45] and Chen et al. [46] focused on tungsten-reinforced cementitious composites, demonstrating improvements in flexural and impact resistance, as well as radiation shielding properties.

In a broader context, water's status as a precious and limited resource accentuates the imperative to develop efficient strategies for anticipating and addressing water loss. Wastewater treatment plants emerge as exceptional tools for curbing water waste and recycling utilized water. However, the corrosive tendencies of wastewater posed a challenge, demanding a solution to mitigate the impact of corrosion. Because of its unique properties, including high density and excellent corrosion and radiation protection, tungsten is particularly interesting for applications in nuclear facilities and infrastructure exposed to extreme environmental conditions. Tungsten is a very promising candidate for the design of

wastewater treatment plant structures, providing protection against the ravages of aggressive water.

Within the purview of this specific inquiry, our primary focus is directed towards an in-depth exploration of the mechanical implications stemming from the introduction of tungsten nanoparticles into the components comprising wastewater treatment plant structures. This comprehensive analysis focuses on the response of these structures to external bending loads, encompassing both static and hydrostatic forces. Utilizing the refined plate theory (RPT), we simulate the WWTP component made of stainless steel analytically. We employ Hamilton's principle to construct the equations of motion for the steel plate, while Navier's analytical solutions provide equilibrium solutions for a simply supported steel panel. Our investigation encompasses critical parameters, including the volume percentage of tungsten nanoparticles seamlessly integrated into the steel matrix. The foundation of the wastewater treatment plant (WWTP) is envisaged as a plate structure, subjected to a uniformly distributed static load originating from the stored water. In tandem, the WWTP structure's walls are postulated as plates, subjected to a linearly varying hydrostatic load. At the surface area, the load is null, whereas at the bottom, it attains its maximum magnitude. Moreover, this research unveils previously unreported outcomes, casting a fresh spotlight on the role of tungsten nanoparticles as enhancers for steel alloy elements.

In essence, by elucidating the mechanical implications of incorporating tungsten nano-sized particles into wastewater treatment plant structures (WWTP), this study breaks new ground by presenting novel results that advance our understanding of materials science in the context of sustainable engineering. By uncovering novel results and exploring the complex interplay between water preservation, structural integrity and innovative materials, our research highlights the potential of tungsten nanoparticles to serve as effective improvers for steel alloying elements. These ideas not only contribute to the current discourse on sustainable engineering practices, but also pave the way for the development of a resilient infrastructure capable of meeting the challenges of wastewater treatment operations.

2. HOMOGENIZATION MODEL

To streamline our analytical approach, we adopt a simplification wherein the components of the wastewater treatment plant are represented as plates. This simplification is particularly pertinent given that corrosion tends to manifest predominantly at the base of the monolithic WWPT structure. In our model, we consider a plate configuration characterized by a simple support arrangement and composed of stainless steel as illustrated in Figure 5.

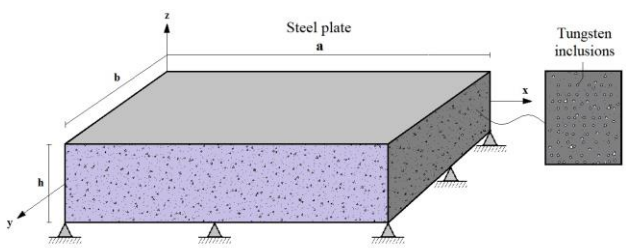

Figure 5. A simply supported steel plate infused with Tungsten nanoparticles

With these assumptions in place, our investigation is directed towards comprehending the mechanical behavior of this element when subjected to the hydrostatic bending loads. This strategic alignment of our study allows us to delve into the intricate interplay between structural integrity, material properties, and loading conditions, yielding valuable insights into the performance of the treated plate in real-world scenarios.

To derive the equivalent elastic properties of a steel matrix infused with varying proportions of nano-sized tungsten particles, we employ the well-established Mori-Tanaka model. This model operates on the premise that each inclusion within the initial infinite matrix experiences an effective stress equal to the average stress exerted on the entire matrix. This methodology enables accurate determination of the effective moduli for composites containing dispersed inclusions, even when these inclusions constitute a substantial volume fraction [47].

One of the pivotal assumptions preceding the application of Mori-Tanaka's homogenization approach is the consideration that the dispersed inclusions possess a uniform physical form. In our specific scenario, the composite containing the steel matrix is reinforced with spherical-shaped tungsten particles distributed randomly in an infinite steel matrix. This assumption greatly facilitates the computation of the homogenized Young's modulus (E_{hom}), Bulk modulus (K_{hom}), and shear modulus (G_{hom}). The expressions for these properties can be defined as follows [47]:

$$\begin{aligned} E_{hom} &= \frac{9K_{hom}G_{hom}}{3K_{hom}+G_{hom}} \\ G_{hom} &= G_A + \frac{V_T G_A (G_T - G_A)}{G_A + \beta_1 (1-V_T)(G_T - G_A)} \\ K_{hom} &= K_A + \frac{V_T K_A (K_T - K_A)}{K_A + \beta_2 (1-V_T)(K_T - K_A)} \end{aligned} \tag{1}$$

where,

$$\begin{aligned} K\alpha &= E\alpha/(3(1-2\nu\alpha)) \\ G\alpha &= E\alpha/(2(1+\nu\alpha)) \end{aligned} \tag{2}$$

In Eq. (2), for the separated isotropic materials (steel and tungsten nanoparticles), the symbols K_α and G_α are denoted by the subscript α, where α represents 'A' when the intended calculation pertains to the steel matrix, and it represents 'T' when the calculated properties are associated with the tungsten reinforcements. These properties are expressed through the well-known conversion formulas for isotropic materials.

For the spherical or ellipsoidal shaped inclusions in a metal matrix the, the correction coefficients β_1 and β_2 are expressed as [47]:

$$\begin{aligned} \beta_1 &= \frac{2(4-5\nu_A)}{15(1-\nu_A)} \\ \beta_2 &= 3 - 5\beta_2 \end{aligned} \tag{3}$$

Taking into account the principle that the volume of a composite, combined with its reinforcement, sums up to unity:

$$V_A + V_T = V_{tot} = 1 \tag{4}$$

The homogenization of Poisson's ratio is governed by Eq. (5), as indicated in [48]:

$$\nu_A V_A + \nu_T V_T = V_{hom} = 1 \tag{5}$$

3. ANALYTICAL MODELLING OF THE STRUCTURE

In conducting this analysis, we embrace the well-established refined plate theory (RPT), a framework that intricately captures both bending and shear elements within the plate thickness [49]. This theory has garnered a track record of precision and reliability, having previously demonstrated its prowess in effectively prognosticating the intricate mechanical responses of composite plates. As an illustration, Zenkour [50] used the refined plate theory to examine the bending behavior of a functionally graded material plate under varying bending loads. Ahmed et al. [51] and Bouamama et al. [52] used it for the dynamic analysis of composite plates and beams respectively. Their findings concluded that the refined plate theory aligns seamlessly with observations and yields notably more accurate outcomes when juxtaposed against the generalized higher-order deformation theory of Reddy [53]. This underscores the efficacy and precision of the refined plate theory in capturing the intricate mechanical nuances of complex plate structures.

3.1 Kinematics

The displacement field of a material point situated at coordinates (x, y, z) within the plate, as governed by the Refined Plate Theory (RPT), can be delineated in the ensuing manner:

$$\begin{gathered} U(x,y,z) = u_0(x,y) - z\frac{\partial w_b(x,t)}{\partial x} + f(z)\frac{\partial w_s(x,y)}{\partial x} \\ V(x,y,z) = v_0(x,y) - z\frac{\partial w_b(x,t)}{\partial y} + f(z)\frac{\partial w_s(x,y)}{\partial y} \\ W(x,y,z) = w_b(x,y) + w_s(x,y) \end{gathered} \tag{6}$$

The shape function expressing shear across the thickness takes the following form [54]:

$$f(z) = sinh^{-1}\left(\frac{3\,z}{h}\right) - z\frac{6}{h\sqrt{13}} \tag{7}$$

The deformation components associated with the utilized refined plate theory are acquired through the following procedure:

$$\begin{gathered} \varepsilon_x = \frac{\partial U}{\partial x};\ \varepsilon_y = \frac{\partial V}{\partial y};\ 2\gamma_{xy} = \frac{\partial U}{\partial y} + \frac{\partial V}{\partial x} \\ 2\gamma_{xz} = \frac{\partial U}{\partial z} + \frac{\partial W}{\partial x};\ 2\gamma_{yz} = \frac{\partial V}{\partial z} + \frac{\partial W}{\partial y} \end{gathered} \tag{8}$$

The constitutive stress-strain relationships for the steel matrix infused with tungsten nanoparticles, are delineated as follows:

$$\begin{Bmatrix} \sigma_x \\ \sigma_y \\ \tau_{xy} \\ \tau_{xz} \\ \tau_{yz} \end{Bmatrix} = \begin{bmatrix} C_{11}^T & C_{12}^T & 0 & 0 & 0 \\ C_{12}^T & C_{22}^T & 0 & 0 & 0 \\ 0 & 0 & C_{66}^T & 0 & 0 \\ 0 & 0 & 0 & C_{44}^T & 0 \\ 0 & 0 & 0 & 0 & C_{55}^T \end{bmatrix} \begin{Bmatrix} \varepsilon_x \\ \varepsilon_y \\ \gamma_{xy} \\ \gamma_{xz} \\ \gamma_{yz} \end{Bmatrix} \tag{9}$$

In this context, C_{ij}^T symbolizes the diminished elastic constants of the amalgamated system, encompassing both the tungsten reinforcement and steel matrix. These constants are established through the application of Mori-Tanaka's homogenization methodology in which:

$$\begin{gathered} C_{11}^T = C_{22}^T = \frac{(1-\upsilon_{hom})E_{hom}}{(1+\upsilon_{hom})(1-2\upsilon_{hom})}; \\ C_{12}^T = \frac{\upsilon E_{hom}}{(1+\upsilon_{hom})(1-2\upsilon_{hom})}; \\ C_{66}^T = C_{55}^T = C_{44}^T = \frac{E_{hom}}{(1+\upsilon_{hom})}. \end{gathered} \tag{10}$$

3.2 Equations of motion

Hamilton's principle is invoked to formulate the equations of motion for the nano-composite plate:

$$\int_0^t (\delta U + \delta V)dt = 0 \tag{11}$$

where, δU and δV correspond to the virtual variations of the internal strain energy within the plate and the external energy induced by the external bending loads, respectively.

The expression for the virtual strain energy imparted by the plate is as follows:

$$\begin{gathered} \delta U = \int_0^A \int_{-h/2}^{h/2} \left(\sigma_x \delta\varepsilon_x + \sigma_y \delta\varepsilon_y + \tau_{xy}\delta\gamma_{xy} + \right. \\ \left. \tau_{yz}\delta\gamma_{yz} + \tau_{xz}\delta\gamma_{xz}\right) dAdz \end{gathered} \tag{12}$$

substituting the strain expression from Eqs. (8)-(9) into Eq. (12), the resultant outcome is as follows:

$$\begin{gathered} \delta U = \int_A \left(N_x \frac{\partial \delta u_0}{\partial x} - M_x^b \frac{\partial^2 \delta w_b}{\partial^2 x} + M_x^s \frac{\partial^2 \delta w_s}{\partial^2 x} + N_y \frac{\partial \delta v_0}{\partial y} - \right. \\ M_y^b \frac{\partial^2 \delta w_b}{\partial^2 y} + M_y^s \frac{\partial^2 \delta w_s}{\partial^2 y} + N_{xy}\left(\frac{\partial \delta u_0}{\partial y} + \frac{\partial \delta v_0}{\partial x}\right) + 2M_x^b \frac{\partial^2 \delta w_b}{\partial x \partial y} + \\ \left. 2M_x^s \frac{\partial^2 \delta w_s}{\partial x \partial y} + Q_{yz}\left(\frac{\partial \delta w_s}{\partial y}\right) + Q_{xz}\left(\frac{\partial \delta w_s}{\partial x}\right)\right) \end{gathered} \tag{13}$$

In Eq. (13), the stress and moment resultants are expressed in the following form:

$$\begin{gathered} N_{ij} = \int_{-h/2}^{h/2} \sigma_{ij} bdz\ ; i,j = x,y \\ M_{ij}^b = \int_{-h/2}^{h/2} z\sigma_{ij} bdz\ ; i,j = x,y \\ M_{ij}^s = \int_{-h/2}^{h/2} f(z)\sigma_{ij} bdz\ ; i,j = x,y \\ Q_{iz} = \int_{-h/2}^{h/2} g(z)\tau_{iz} bdz\ ; i = x,y \end{gathered} \tag{14}$$

In the case of the nano-reinforced steel plate experiencing mechanical bending loads denoted as 'q', the virtual external work engendered by these loads is defined by Equation.

$$\delta V = -\int_A \int_{-h/2}^{h/2} q(\delta w_b + \delta w_s)\, dAdz \tag{15}$$

By employing Eqs. (13) and (15), within Eq. (11), and subsequently performing integration by parts while accounting for the coefficients of δu_0, δv_0, δw_b, and δw_s, the resulting equations of motion pertinent to the refined plate theory are derived as follows:

$$\begin{gathered} \delta u_0 : \frac{\partial N_x}{\partial x} + \frac{\partial N_{xy}}{\partial y} = 0 \\ \delta v_0 : \frac{\partial N_y}{\partial y} + \frac{\partial N_{xy}}{\partial x} = 0 \\ \delta w_b : \left(\frac{\partial^2 M_x^b}{\partial x^2} - 2\frac{\partial^2 M_{xy}^b}{\partial x \partial y} + \frac{\partial^2 M_y^b}{\partial y^2}\right) + q = 0 \\ \delta w_s : \left(\frac{\partial^2 M_x^s}{\partial x^2} - 2\frac{\partial^2 M_x^s}{\partial x \partial y} + \frac{\partial^2 M_y^s}{\partial y^2}\right) + \left(\frac{\partial Q_{xz}}{\partial x} + \frac{\partial Q_{yz}}{\partial y}\right) + \\ q = 0 \end{gathered} \tag{16}$$

3.3 Navier's solutions for simply supported plates

Contemplate a rectangular steel plate (as depicted in Figure 5), which is simply supported. The boundary conditions for a simply supported steel plate reinforced with spherical shaped tungsten nanoparticles are defined as follows:

$$\begin{matrix} x = 0\ and\ x = a : v_0 = w_b = w_s = N_x = M_x^b = M_x^s = 0 \\ y = 0\ and\ y = b : u_0 = w_b = w_s = N_y = M_y^b = M_y^s = 0 \end{matrix} \quad (17)$$

The admissible displacement functions according to Navier, expressed as trigonometric series and fulfilling the boundary conditions outlined in Eq. (17), are presented as follows:

$$\begin{matrix} u(x,y) = \sum_{n=1}^{\infty}\sum_{m=1}^{\infty} U_{mn} cos(\lambda x)\, sin(\mu y) \\ v(x,y) = \sum_{n=1}^{\infty}\sum_{m=1}^{\infty} V_{mn} sin(\lambda x)\, cos(\mu y) \\ w_b(x,y) = \sum_{n=1}^{\infty}\sum_{m=1}^{\infty} W_{bmn} sin(\lambda x)\, sin(\mu y) \\ w_s(x,y) = \sum_{n=1}^{\infty}\sum_{m=1}^{\infty} W_{smn} sin(\lambda x)\, sin(\mu y) \end{matrix} \quad (18)$$

here, (U_{mn}, V_{mn}, W_{bmn}, W_{smn}) are the arbitrary parameters to be determined. where, λ=mπ/a and μ=nπ/b. For the ensuing outcomes, an increased number of iterations (n=201, m=201) was employed to achieve greater precision and accuracy in the results. This decision was based on the available computational resources, enabling more comprehensive calculations and enhanced precision.

In our analysis, we posit that the transverse bending load "q" manifests as hydrostatical forms, as illustrated in Figure 6. These bending loads can be effectively represented through the utilization of the Double-Fourier series, as depicted below:

$$q(x,y) = \sum_{m=1}^{\infty}\sum_{n=1}^{\infty} Q_{mn}\, sin(\lambda x) sin(\mu x) \quad (19)$$

where,

$$Q_{mn} = \left\{ \frac{8q_0}{mn\pi^2} cos(m\pi) \right. \quad (20)$$

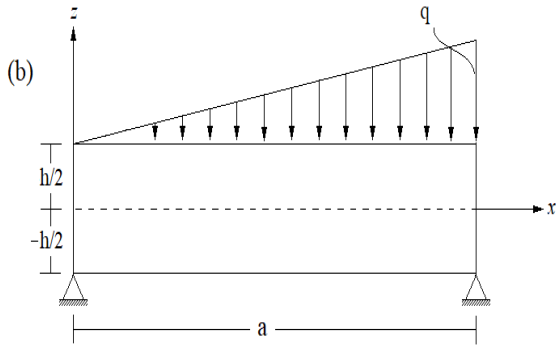

Figure 6. Simply supported steel plate subjected to external bending linear hydrostatic load

Ultimately, to attain the analytical solutions, the outcomes of the substitution can be organized into the subsequent matrix format:

$$\begin{bmatrix} k_{11} & k_{12} & k_{13} & k_{14} \\ k_{21} & k_{22} & k_{23} & k_{24} \\ k_{31} & k_{32} & k_{33} & k_{34} \\ k_{41} & k_{42} & k_{43} & k_{44} \end{bmatrix} \begin{Bmatrix} U_{mn} \\ V_{mn} \\ W_{bmn} \\ W_{smn} \end{Bmatrix} = \begin{Bmatrix} 0 \\ 0 \\ Q_{mn} \\ Q_{mn} \end{Bmatrix} \quad (21)$$

where,

$$\begin{matrix} k_{11} = -A_{11}\lambda^2 - A_{66}\mu^2;\ k_{12} = -\lambda\mu(A_{66} + A_{12}); \\ k_{13} = B_{11}\lambda^3 + (2B_{66} + B_{12})\lambda\mu^2; \\ k_{14} = B_{s11}\lambda^3 + (2B_{s66} + B_{s12})\lambda\mu^2 \\ k_{21} = k_{12};\ k_{22} = -(A_{11}\lambda^2 + A_{66}\mu^2); \\ k_{23} = B_{22}\mu^3 + (2B_{66} + B_{12})\lambda^2\mu; \\ k_{24} = B_{s22}\mu^3 + (2B_{s66} + B_{s12})\lambda^2\mu; \\ k_{31} = k_{13}\ ;\ k_{32} = k_{23}\ ; \\ k_{33} = -D_{11}\lambda^4 + 2\lambda^2\mu^2(D_{12} + 2D_{66}) + D_{22}\mu^4; \\ k_{34} = -D_{s11}\lambda^4 + 2\lambda^2\mu^2(D_{s12} + 2D_{s66}) + D_{s22}\mu^4; \\ k_{41} = k_{14}\ ;\ k_{42} = k_{24}\ ;\ k_{43} = k_{34}\ ; \\ k_{44} = -A_{ss11}\lambda^4 - 2\lambda^2\mu^2(A_{ss12} + 2A_{ss66}) \\ + A_{ss22}\mu^4 + A_{cc55}\lambda^2 + A_{cc44}\mu^2; \end{matrix} \quad (22)$$

$$\begin{matrix} \{A, B, D, A_s, B_s, A_{ss}\} = \\ \int_{-h/2}^{\frac{h}{2}} \{1, z, z^2, f(z), zf(z), f(z)^2\}\, C_{ij}^T bdze \\ \{A_{cc}\} = \int_{-h/2}^{h/2} \{g(z)^2\}\, C_{ij}^T bdz \end{matrix} \quad (23)$$

4. RESULTS AND DISCUSSION

This section offers a captivating exploration into the mechanical bending behavior of steel plates enriched with an array of tungsten nanoplatelets. As indicated by Chen et al. [55], the Young's modulus for steel falls within the range of E_A=[200-210] GPa, while the modulus for tungsten nanoparticles is E_T=[400-450] GPa. For our analysis, we've chosen a stainless-steel matrix featuring a Young's modulus of E_A=200 GPa, reinforced with tungsten nanoparticles possessing a Young's modulus of E_T=400 GPa. The respective Poisson ratios are v_A=0.33 for steel and v_T=0.28 for the reinforcement.

$$\begin{matrix} \overline{w} = \frac{10^2 E_A h^3}{q_0 a^4} w\left(\frac{a}{2}, \frac{b}{2}, z\right). \\ \overline{U} = \frac{10^2 E_A h^3}{q_0 a^4} u\left(0, \frac{b}{2}, z\right). \\ \sigma_x(z) = \frac{h}{q_0 a} \sigma_x^0\left(\frac{a}{2}, \frac{b}{2}, z\right). \\ \tau_{xy}(z) = \frac{h}{q_0 a} \tau_{xy}^0(0, 0, z). \\ \tau_{xz}(z) = \frac{h}{q_0 a} \tau_{xz}^0\left(0, \frac{b}{2}, z\right). \end{matrix} \quad (24)$$

Within this section, we harness the refined plate deformation theory to intricately calculate transverse displacements ($\overline{w}$), axial displacement ($\overline{U}$), and normal and shear stresses (σ_x, σ_y, τ_{xz}, τ_{yz}, τ_{xy}). These comprehensive analyses yield a collection of dimensionless Eq.(24), which serve to not only facilitate the interpretation of results but also enable their visualization through numerical and graphical representations. By employing these equations, we delve into a profound exploration of the hydrostatic behavior exhibited by the plates, thereby enriching our comprehension of their mechanical response.

4.1 Steel-tungsten nano-composite elastic properties

To initiate, it is highly advantageous to visually depict the consequences resulting from the integration of varying proportions of tungsten nanoparticles using Mori-Tanaka's

approach, in relation to the elastic properties of the steel nano-composite plate. This illustrative representation is conveniently presented in Table 1, which systematically outlines the effects of different entities, ranging from 5% to 30% of the total volume percentage of the steel matrix.

Table 1. The effective mechanical properties of the mixture

V_T (Vt%)	5%	10%	20%	30%
E_{hom} (GPa)	210.11	220.20	240.33	260.40
ν_{hom}	0.328	0.325	0.320	0.315
G_{hom} (GPa)	77.22	83.25	91.32	99.40
K_{hom} (GPa)	201.43	206.79	217.50	228.20

Table 1 clearly demonstrates that the incorporation of tungsten nanoparticle reinforcement exerts a strengthening influence on the steel matrix. It is evident that the constants (E_{hom}, G_{hom}, K_{hom}) characterizing the elastic properties of the impregnated steel rises proportionally with the concentration of the reinforcement (V_T). Interestingly, as the percentage of tungsten particles increases, so do the elastic properties of the composite, reaching an optimal peak at the 30% concentration. At this concentration, the elastic modulus (E_{hom}) of the stainless-steel matrix can be enhanced by 30%, while the shear (G_{hom}) and bulk (K_{hom}) modulus of the stainless steel can increase by 28%. This enhancement can be attributed to the exceptional elastic properties inherent to tungsten nanoparticles.

To establish the credibility of our material characterization involving stainless steel enriched with tungsten nanoparticles, it's crucial to conduct a comprehensive comparative study of the nanocomposite's estimated elastic properties.

This comparative analysis serves two main purposes: validating the analytical homogenization model, particularly the Mori-Tanaka model, and confirming the calculated equivalent elastic properties of the nanocomposite. Our study includes a comparison of the estimated elastic moduli (E_{tot}) for a steel matrix reinforced with nano-sized tungsten particles using both the Mori-Tanaka and Eshelby homogenization models [56]. Furthermore, we integrate the Hashin and Shtrikman [57] (HS) model into our comparative study to provide a full range of values and define limiting parameters.

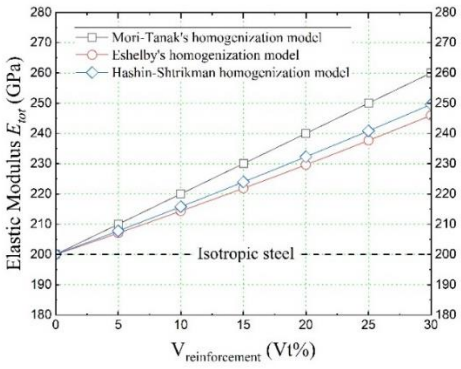

Figure 7. Comparative analysis of elastic moduli (E_{tot}) of a steel matrix infused with tungsten naoparticles utilizing analytical homogenization models

Figure 7 illustrates the collective elastic moduli of a steel plate infused with tungsten nanoparticles using three distinct homogenization models. It is evident from Figure 7 that there is a consistent increase in elastic constants (E_{tot}) with the incorporation of tungsten nanoparticles, regardless of the homogenization model used in the analysis. This observed enhancement in elastic properties can be directly attributed to the high elastic properties of tungsten particles. However, subtle variations in the estimated elastic constants are noticeable, likely stemming from the different assumptions inherent to each model. Specifically, Mori-Tanaka's model, which assumes a perfectly spherical shape for the nanoparticles, may account for some of these variations.

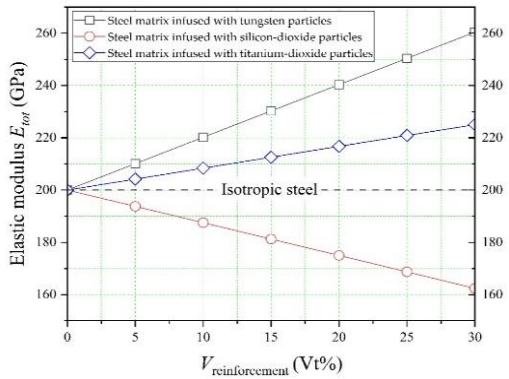

Figure 8. Comparative analysis of reinforcement effects on steel matrix: tungsten, silicon oxide, and titanium oxide infusions utilizing Mori-Tanaka's approach

To contrast the impact of incorporating tungsten reinforcement particles within a steel matrix, a comparative analysis is presented in Figure 8 alongside other reinforcements, namely silicon oxide and titanium oxide, which are similarly infused into a steel matrix. The Mori-Tanaka's approach is employed for this comparative study.

The advantageous effect of tungsten reinforcement becomes evident when comparing it to other reinforcements, as Figure 8 illustrates. The discernible prominence of tungsten particles in enhancing elastic constants of the composite stands out, showing a more pronounced impact compared to the other substances, namely, silicon dioxide and titanium dioxide.

4.2 Hydrostatic bending analysis of the structure

In wastewater treatment plants (WWTP) structures, the accumulated used water within the structure imposes a hydrostatic bending load on its walls. Consequently, the ensuing section entails an analysis aimed at investigating the impact of linearly distributed loads (see Figure 6). These loads are null at the water surface and reach their maximum magnitude at the base of the structure. For the purposes of this analysis, the walls of the structure are considered as plates.

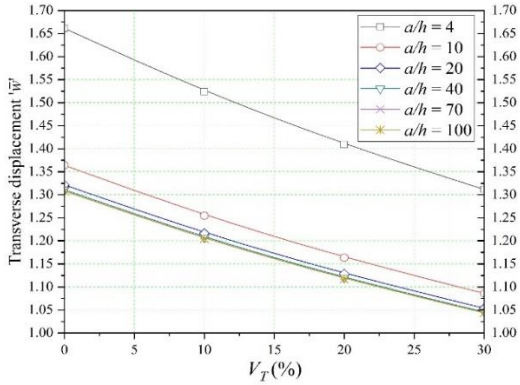

Figure 9. Impact of thickness-to-length ratio on tungsten reinforced steel plate under hydrostatic loading (a=b)

Figure 9 illustrates the effect of thickness-to-length ratio on a steel plate, reinforced with varying proportions of tungsten nanoparticles and subjected to hydrostatic loading. Notably, the observation reveals that the maximum transverse displacement occurs in a non-reinforced steel plate. In contrast, the minimum transverse displacement is consistently observed at a 30% volume fraction of reinforcement, irrespective of the length-to-thickness ratios. However, regardless of the thickness-to-length ratio (*a/b*), tungsten nano-sized particles consistently exhibit the same level of reinforcement effect.

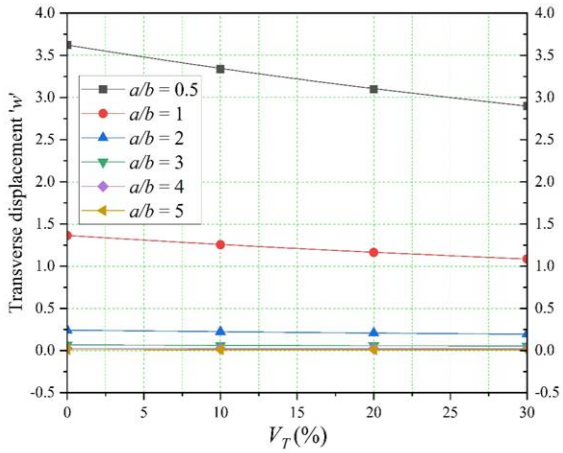

Figure 10. Influence of length-to-width ratio on tungsten reinforced steel plate under linearly distributed hydrostatic load (a/h = 10)

Figure 10 presents the impact of length-to-width ratio on a steel plate, reinforced with varying proportions of tungsten particles, and exposed to linearly distributed hydrostatic load. Notably, the discernible effect of tungsten particles, contributing to reinforcement, becomes more pronounced at reduced geometric ratios. As previously mentioned, regardless of the aspect ratio, tungsten maintains its strengthening effect, consistently enhancing the flexural strength of the plate.

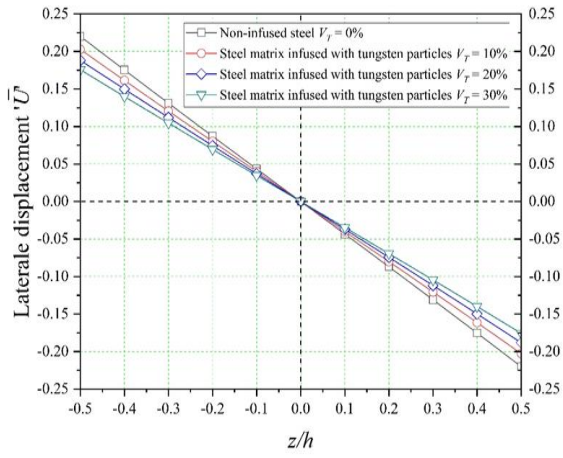

Figure 11. Hydrostatic bending load effect on axial displacement of tungsten reinforced steel plate (a=b, a/h=10)

Depicts the influence of hydrostatic bending load on the axial displacement of a steel plate, strengthened with diverse proportions of tungsten nanoparticles. Outcomes in Figure 11 affirm that tungsten reinforcement not only diminishes transverse displacement but also reduces axial displacement in the plate. Specifically, the lower axial displacement is notably evident when the volume of tungsten within the steel matrix reaches 30% , resulting in a decrease in axial displacement of approximately 26%.

Table 2. Normal stresses (σ_x, σ_y) of an advanced composite plate under hydrostatic load

Plate Stress	V_T (%)	Length-to Thickness Ratio (a/h)			
		a/h=4	a/h=10	a/h=20	a/h=100
Normal stress (σ_x, σ_y)	0	-0,527	-1,297	-2,588	-12,930
	10	-0,521	-1,281	-2,557	-12,774
	20	-0,514	-1,266	-2,526	-12,621
	30	-0,508	-1,251	-2,496	-12,472

Table 3. Dimensionless transverse shear stresses $\tau_{xz}, \tau_{yz}, \tau_{xy}$ of different steel plates subjected to hydrostatic load, considering different proportions of tungsten inclusions

Plate Stress	V_T (%)	Length-to Thickness Ratio (a/h)			
		a/h=4	a/h=10	a/h=20	a/h=100
Shear stress (τ_{xy})	0	-0,494	-1,161	-2,297	-11,441
	10	-0,502	-1,181	-2,338	-11,643
	20	-0,510	-1,201	-2,377	-11,840
	30	-0,517	-1,220	-2,415	-12,032
Transverse shear stress (τ_{xz}, τ_{yz})	0	0,8950	0,9063	0,9097	0,9114
	10	0,8952	0,9064	0,9097	0,9114
	20	0,8954	0,9065	0,9098	0,9114
	30	0,8955	0,9065	0,9098	0,9114

At last, Tables 2 and 3 comprehensively outlines the impact of distinct tungsten reinforcement proportions within the steel matrix, coupled with varying geometric aspect ratios (a/h), on the normal and shear stresses experienced by the WWPT steel plate. Similar to observations noted earlier for a plate subjected to static behavior, when applying a hydrostatic, an increase in the volume proportions of reinforcement leads to elevated normal stresses, while the shear and transverse shear stresses decrease proportionally with the reinforcement volume.

The evident reduction in shear stresses can be attributed to the enhanced elastic properties, achieved within the steel composite matrix through the integration of tungsten nano-reinforcements. This concurrent decrease in shear and transverse shear stresses across the plate thickness underscores the pivotal role played by tungsten nanoparticles in redistributing stresses within the WWPT steel plate component regardless of the external loading type.

5. CONCLUSIONS

Water is an invaluable resource, vital for human consumption and crucial in sustaining agricultural irrigation. As the need for efficient water management intensifies, Wastewater Treatment Plants (WWTPs) emerge as pivotal solutions, effectively recycling used water. However, safeguarding the integrity of these WWTP structures becomes paramount. Not only must they withstand chemical attacks to ensure water quality, but their mechanical resilience also demands attention. By fortifying WWTPs against both chemical and mechanical threats, we secure a sustainable future for water resources, fostering a resilient environment for generations to thrive.

Hence, our study casts a spotlight on the profound ramifications of introducing tungsten nanoparticles into the mechanical framework of WWPT steel components. In our comprehensive exploration, we meticulously examined an array of critical parameters. These encompassed the manipulation of tungsten reinforcement volume proportions within the steel matrix – a fundamental element of the monolithic structure. Our investigation also entailed a meticulous analysis of geometric ratios inherent in the plate configuration. Furthermore, we methodically evaluated the responses of these components under diverse bending conditions, encompassing the hydrostatic loads.

Our research has yielded a compelling array of insights, each serving to underscore the pivotal significance of our findings:

(1) Introducing nano-sized tungsten into a stainless-steel matrix leads to notable enhancements in elastic characteristics of the composite, encompassing Young's modulus, bulk modulus, and shear modulus. The extent of improvement is intricately linked to the volume concentration of these additives.

(2) The incorporation of an optimal volume of tungsten, precisely evaluated at 30%, into a steel matrix yields remarkable improvement. This improvement elevates the elastic constants 'Etot' of the composite by an impressive 31%, in stark comparison to a steel matrix infused with 30% titanium dioxide, which registers an improvement of up to 13%.

(3) Wastewater treatment plant structures fortified with nano-tungsten particles manifest an exceptional capacity to optimize their response against external mechanical loads. This reinforcement markedly enhances their flexural strength and overall performance.

(4) Under hydrostatic external bending loads, steel plates reinforced with tungsten nanoplatelets exhibit a striking reduction in transverse displacement. This reduction accentuates the effectiveness of nano-reinforcements in curtailing structural deformations across diverse external mechanical loading scenarios.

(5) By introducing 30% of tungsten particles into the steel matrix, transverse displacement experiences a noteworthy decrease of 26%, while axial displacement diminishes by 25%.

(6) Beyond their corrosion-resistant properties, tungsten particles exhibit an additional layer of mechanical advantages, further enhancing their pivotal role in structural optimization.

Whilst this paper focuses on the analytical analysis of the hydrostatic bending of the panels of a wastewater treatment plant made of a new advanced composite tungsten steel material, it offers significant theoretical contributions that will advance the field of nanotechnology in general and nanomaterials in particular, as well as structural engineering, nevertheless the authors acknowledge the limitations of plate theories, particularly regarding the linear elasticity assumption. Plate theories typically rely on the assumption of linear elasticity, which implies that materials behave linearly under loading conditions. As we strive to extend our research further, we recognize the importance of addressing non-linear deformation assumptions. Future investigations will aim to overcome these limitations by incorporating non-linear deformation models to provide more accurate predictions of plate behavior under various loading conditions.

ACKNOWLEDGMENT

The Thematic Agency for Research in Science and Technology (ATRST) of Algiers, Algeria is gratefully acknowledged.

REFERENCES

[1] Elmeddahi, Y., Mahmoudi, H., Issaadi, A., Goosen, M.F., Ragab, R. (2016). Evaluating the effects of climate change and variability on water resources: A case study of the Cheliff Basin in Algeria. American Journal of Engineering and Applied Sciences, 9(4): 835-845. https://doi.org/10.3844/ajeassp.2016.835.845

[2] Boudiaf, B., Dabanli, I., Boutaghane, H., Şen, Z. (2020). Temperature and precipitation risk assessment under climate change effect in northeast Algeria. Earth Systems and Environment, 4: 1-14. https://doi.org/10.1007/s41748-019-00136-7

[3] Sahnoune, F., Belhamel, M., Zelmat, M., Kerbachi, R. (2013). Climate change in Algeria: vulnerability and strategy of mitigation and adaptation. Energy Procedia, 36: 1286-1294. https://doi.org/10.1016/j.egypro.2013.07.145

[4] Bouznit, M., Elaguab, M., Selt, M.M., Himrane, M., Aïssaoui, R. (2022). Climate change and agricultural production in Algeria. Climate Change in the Mediterranean and Middle Eastern Region, 249-268. https://doi.org/10.1007/978-3-030-78566-6_12

[5] Benhamrouche, A., Boucherf, D., Hamadache, R., Bendahmane, L., Martin-Vide, J., Teixeira Nery, J. (2015). Spatial distribution of the daily precipitation concentration index in Algeria. Natural Hazards and Earth System Sciences, 15(3): 617-625. https://doi.org/10.5194/nhess-15-617-2015

[6] Babaousmail, H., Hou, R., Ayugi, B., Gnitou, G.T. (2019). Evaluation of satellite-based precipitation estimates over Algeria during 1998–2016. Journal of Atmospheric and Solar-Terrestrial Physics, 195: 105139. https://doi.org/10.1016/j.jastp.2019.105139

[7] Drouiche, N., Ghaffour, N., Naceur, M.W., Lounici, H., Drouiche, M. (2012). Towards sustainable water management in Algeria. Desalination and Water Treatment, 50(1-3): 272-284. https://doi.org/10.1080/19443994.2012.719477

[8] Alvarez-Ayuso, E., Garcıa-Sánchez, A., Querol, X. (2003). Purification of metal electroplating waste waters using zeolites. Water Research, 37(20): 4855-4862. https://doi.org/10.1016/j.watres.2003.08.009

[9] An, W., Li, X., Ma, J., Ma, L. (2023). Advanced treatment of industrial wastewater by ozonation with iron-based monolithic catalyst packing: From mechanism to application. Water Research, 235: 119860. https://doi.org/10.1016/j.watres.2023.119860

[10] Gürbilek, N. (2013). Nanotechnology in civil infrastructure. Journal of Chemical Information and Modeling, 53.

[11] Huseien, G.F., Khalid, N.H.A., Mirza, J. (2022). Nanotechnology for Smart Concrete. CRC Press. https://doi.org/10.1201/9781003196143

[12] Liu, C., Su, X., Wu, Y., Zheng, Z., Yang, B. (2021). Effect of nano-silica as cementitious materials-reducing admixtures on the workability, mechanical properties

and durability of concrete. Nanotechnology Reviews, 10(1): 1395-1409. https://doi.org/doi:10.1515/ntrev-2021-0097
[13] Chatbi, M., Krour, B., Benatta, M.A., Harrat, Z.R., Amziane, S., Bouiadjra, M.B. (2022). Bending analysis of nano-SiO2 reinforced concrete slabs resting on elastic foundation. Structural Engineering and Mechanics, An Int'l Journal, 84(5): 685-697. https://doi.org/10.12989/SEM.2022.84.5.685
[14] Joshaghani, A., Balapour, M., Mashhadian, M., Ozbakkaloglu, T. (2020). Effects of nano-Tio2, nano-Al2o3, and nano-Fe2o3 on rheology, mechanical and durability properties of self-consolidating concrete (Scc): An experimental study. Construction and Building Materials, 245: 118444-118444. https://doi.org/10.1016/J.CONBUILDMAT.2020.118444
[15] Abu-Okail, M., Alsaleh, N.A., Farouk, W., Elsheikh, A., Abu-Oqail, A. (2021). Effect of Dispersion of alumina nanoparticles and graphene nanoplatelets on microstructural and mechanical characteristics of hybrid carbon/glass fibers reinforced polymer composite. Journal of Materials Research and Technology, 14: 2624-2637. https://doi.org/10.1016/j.jmrt.2021.07.158
[16] Nazari, A., Riahi, S. (2010). The effects of zro2 nanoparticles on physical and mechanical properties of high strength self compacting concrete. Materials Research, 13(1): 551-556. https://doi.org/10.1590/S1516-14392010000400019
[17] Guo, M.Z., Ling, T.C., Poon, C.S. (2013). Nano-Tio2-based architectural mortar for no removal and bacteria inactivation: Influence of coating and weathering conditions. Cement and Concrete Composites, 36(1): 101-108. https://doi.org/10.1016/J.CEMCONCOMP.2012.08.006
[18] Mohajerani, A., Burnett, L., Smith, J.V., Kurmus, H., Milas, J., Arulrajah, A., Horpibulsuk, S., Abdul Kadir, A. (2019). Nanoparticles in construction materials and other applications, and implications of nanoparticle use. Materials, 12(19): 3052. https://doi.org/10.3390/ma12193052
[19] Du, S., Wu, J., AlShareedah, O., Shi, X. (2019). Nanotechnology in cement-based materials: A review of durability, modeling, and advanced characterization. Nanomaterials, 9(9): 1213. https://doi.org/10.3390/nano9091213
[20] Harrat, Z.R., Chatbi, M., Krour, B., Hadzima-Nyarko, M., Radu, D., Amziane, S., Bachir Bouiadjra, M. (2023). Modeling the thermoelastic bending of ferric oxide (Fe2O3) nanoparticles-enhanced RC slabs. Materials, 16(8): 3043. https://doi.org/https://doi.org/10.3390/ma16083043
[21] Benfrid, A., Benbakhti, A., Harrat, Z.R., Chatbi, M., Krour, B., Bouiadjra, M.B. (2023). Thermomechanical analysis of glass powder based eco-concrete panels: Limitations and performance evaluation. Periodica Polytechnica Civil Engineering, 67(4): 1284-1297. https://doi.org/10.3311/PPci.22781
[22] Chatbi, M., Harrat, Z.R., Ghazoul, T., Bouiadjra, M.B. (2022). Free vibrational analysis of composite beams reinforced with randomly aligned and oriented carbon nanotubes, resting on an elastic foundation. Journal of Building Materials and Structures, 9(1): 22-32. https://doi.org/https://doi.org/10.34118/jbms.v9i1.1895
[23] Chatbi, M., Harrat, Z.R., Benatta, M.A., Krour, B., Hadzima-Nyarko, M., Işık, E., Czarnecki, S., Bouiadjra, M.B. (2023). Nano-clay platelet integration for enhanced bending performance of concrete beams resting on elastic foundation: An analytical investigation. Materials, 16(14): 5040. https://doi.org/https://doi.org/10.3390/ma16145040
[24] Long, W.J., Wei, J.J., Xing, F., Khayat, K.H. (2018). Enhanced dynamic mechanical properties of cement paste modified with graphene oxide nanosheets and its reinforcing mechanism. Cement and Concrete Composites, 93: 127-139. https://doi.org/10.1016/j.cemconcomp.2018.07.001
[25] Behzadian, R., Shahrajabian, H. (2019). Experimental study of the effect of nano-silica on the mechanical properties of concrete/PET Composites. KSCE Journal of Civil Engineering, 23(8): 3660-3668. https://doi.org/10.1007/s12205-019-2440-9
[26] Wang, X.F., Huang, Y.J., Wu, G.Y., Fang, C., Li, D.W., Han, N.X., Xing, F. (2018). Effect of nano-SiO2 on strength, shrinkage and cracking sensitivity of lightweight aggregate concrete. Construction and Building Materials, 175: 115-125. https://doi.org/10.1016/j.conbuildmat.2018.04.113
[27] Zhang, P., Sha, D., Li, Q., Zhao, S., Ling, Y. (2021). Effect of nano silica particles on impact resistance and durability of concrete containing coal fly ash. Nanomaterials, 11(5): 1296. https://doi.org/10.3390/nano11051296
[28] Bhatta, D.P., Singla, S., Garg, R. (2022). Experimental investigation on the effect of Nano-silica on the silica fume-based cement composites. Materials Today: Proceedings, 57: 2338-2343. https://doi.org/10.1016/j.matpr.2022.01.190
[29] McCall, W.R. (2014). Piezoelectric Nanoparticle-Polymer Composite Materials. University of California, San Diego.
[30] Magnani, A., Capaccioli, S., Azimi, B., Danti, S., Labardi, M. (2022). Local piezoelectric response of polymer/ceramic nanocomposite fibers. Polymers, 14(24): 5379. https://doi.org/10.3390/polym14245379
[31] Rashid, A.B., Hoque, M.E. (2022). Polymer nanocomposites for defense applications. In Advanced Polymer Nanocomposites, pp. 373-414. https://doi.org/10.1016/B978-0-12-824492-0.00015-5
[32] Rashid, A.B., Haque, M., Islam, S.M., Labib, K.R.U. (2024). Nanotechnology-enhanced fiber-reinforced polymer composites: Recent advancements on processing techniques and applications. Heliyon, 10: e24692. https://doi.org/10.1016/j.heliyon.2024.e24692
[33] Yuvaraj, G., Ramesh, M., Rajeshkumar, L. (2023). Carbon and cellulose-based nanoparticle-reinforced polymer nanocomposites: A critical review. Nanomaterials, 13(11): 1803. https://doi.org/10.3390/nano13111803
[34] Mohammadpour, Z., Zare, H.R. (2020). Improving the corrosion resistance of the nickel–tungsten alloy by Optimization of the electroplating conditions. Transactions of the Indian Institute of Metals, 73(4): 937-944. https://doi.org/10.1007/s12666-020-01894-z
[35] Bentur, A., Berke, N., Diamond, S. (1997). Steel Corrosion On Concrete: Fundamentals and civil engineering practice. CRC press. https://doi.org/10.1201/9781482271898

[36] Burkov, A.A., Chigrin, P.G. (2018). Effect of tungsten, molybdenum, nickel and cobalt on the corrosion and wear performance of Fe-based metallic glass coatings. Surface and Coatings Technology, 351: 68-77. https://doi.org/10.1016/j.surfcoat.2018.07.078
[37] Nishimura, T., Noda, K., Kodama, T. (2001). Corrosion behavior of tungsten-bearing steel in a wet/dry environment containing chloride ions. Corrosion, 57(09): NACE-01090753.
[38] Liu, C., Xu, M., Zhang, W., Pu, S., Chu, P.K. (2008). Effects of tungsten pre-implanted layer on corrosion and electrochemical characteristics of amorphous carbon films on stainless steel. Diamond and Related Materials, 17(7-10): 1738-1742. https://doi.org/10.1016/j.diamond.2008.01.114
[39] Xavier, J.R. (2022). Superior surface protection, mechanical and hydrophobic properties of silanized tungsten carbide nanoparticles encapsulated epoxy nanocomposite coated steel structures in marine environment. Silicon, 14(17): 11147-11161. https://doi.org/10.1007/s12633-022-01842-0
[40] Ali, L.F., Kuppuswamy, N., Soundararajan, R., Ramkumar, K.R., Sivasankaran, S. (2021). Microstructural evolutions and mechanical properties enhancement of AA 6063 alloy reinforced with Tungsten (W) nanoparticles processed by friction stir processing. Materials Characterization, 172: 110903. https://doi.org/10.1016/j.matchar.2021.110903
[41] Lu, T., Chen, C., Li, P., Zhang, C., Han, W., Zhou, Y., Suryanarayana, C., Guo, Z. (2021). Enhanced mechanical and electrical properties of in situ synthesized nano-tungsten dispersion-strengthened copper alloy. Materials Science and Engineering: A, 799: 140161. https://doi.org/10.1016/j.msea.2020.140161
[42] Bartkowski, D., Bartkowska, A., Popielarski, P., Hajkowski, J., Piasecki, A. (2020). Characterization of W–Cr metal matrix composite coatings reinforced with WC particles produced on low-carbon steel using laser processing of precoat. Materials, 13(22): 5272. https://doi.org/10.3390/ma13225272
[43] Dong, L.L., Fu, Y.Q., Liu, Y., Lu, J.W., Zhang, W., Huo, W.T., Jin, J.H., Zhang, Y.S. (2021). Interface engineering of graphene/copper matrix composites decorated with tungsten carbide for enhanced physico-mechanical properties. Carbon, 173: 41-53. https://doi.org/10.1016/j.carbon.2020.10.091
[44] Zhang. L., Jiang, Y., Fang, Q, Xie, Z., Miao, S., Zeng, L., Zhang, T., Wang, X., Liu, C. (2017). Microstructure and mechanical properties of tungsten composite reinforced by fibre network. Frontiers of Materials Science, 11: 190-196. https://doi.org/10.1007/s11706-017-0378-8
[45] Liu, X., Lian, Y.Y., Greuner, H., Boeswirth, B., Jin, Y.Z., Feng, F., Wang, J.B., Chen, L., Song, J.P., Yu, Y., Zhang, T., Liu, C.S., Tan, J., Liu, D.P., Duan, X.R. (2017). Irradiation effects of hydrogen and helium plasma on different grade tungsten materials. Nuclear Materials and Energy, 12: 1314-1318. https://doi.org/10.1016/j.nme.2017.01.018
[46] Chen, G., Luo, T., Shen, S., Zheng, J., Tang, X., Tao, T., Xue, W. (2021). Tungsten particles reinforced high-entropy alloy matrix composite prepared by in-situ reaction. Journal of Alloys and Compounds, 862: 158037. https://doi.org/10.1016/j.jallcom.2020.158037
[47] Mori, T., Tanaka, K. (1973). Average stress in matrix and average elastic energy of materials with misfitting inclusions. Acta metallurgica, 21(5): 571-574. https://doi.org/10.1016/0001-6160(73)90064-3
[48] Theocaris, P.S., Stavroulakis, G.E. (1998). The homogenization method for the study of variation of Poisson's ratio in fiber composites. Archive of Applied Mechanics, 68: 281-295. https://doi.org/10.1007/s004190050165
[49] Vo, T.P., Thai, H.T., Nguyen, T.K., Inam, F. (2014). Static and vibration analysis of functionally graded beams using refined shear deformation theory. Meccanica, 49: 155-168. https://doi.org/10.1007/s11012-013-9780-1
[50] Zenkour, A.M. (2013). A simple four-unknown refined theory for bending analysis of functionally graded plates. Applied Mathematical Modelling, 37(20-21): 9041-9051. https://doi.org/10.1016/j.apm.2013.04.022
[51] Ahmed, B., Fouad, B., Djalil, B.A., Mohamed, B.B., Abdelouahed, T., Bedia, E.A. (2016). The thermal study of wave propagation in functionally graded material plates (FGM) based on neutral surface position. Mathematical Modelling of Engineering Problems, 3(4): 202-205. https://doi.org10.18280/mmep.030410
[52] Bouamama, M., Elmeiche, A., Elhennani, A., Kebir, T., Harchouche, Z.E.A. (2020). Exact solution for free vibration analysis of FGM beams. Revue des Composites et des Matériaux Avancés, 30(2): 55-60. https://doi.org/10.18280/rcma.300201
[53] Reddy, J.N. (1984). A simple higher-order theory for laminated composite plates. Journal of Applied Mechanics, 51(4): 745-752. https://doi.org/10.1115/1.3167719
[54] Benbakhti, A., Bouiadjra, M.B., Retiel, N., Tounsi, A. (2016). A new five unknown quasi-3D type HSDT for thermomechanical bending analysis of FGM sandwich plates. Steel and Composite Structures, 22(5): 975-999. https://doi.org/10.12989/scs.2016.22.5.975
[55] Chen, Z., Gandhi, U., Lee, J., Wagoner, R.H. (2016). Variation and consistency of Young's modulus in steel. Journal of Materials Processing Technology, 227: 227-243. https://doi.org/10.1016/j.jmatprotec.2015.08.024
[56] Eshelby, J.D. (1957). The determination of the elastic field of an ellipsoidal inclusion, and related problems. Proceedings of the Royal Society of London. Series A. Mathematical and Physical Sciences, 241(1226): 376-396. https://doi.org/10.1098/rspa.1957.0133
[57] Hashin, Z., Shtrikman, S. (1962). A variational approach to the theory of the effective magneticpermeability of multiphase materials. Journal of Applied Physics, 33(10): 3125-3131. https://doi.org/10.1063/1.1728579

NOMENCLATURE

E	the elasticity modulus
G	the shear modulus
K	the bulks modulus
V	the volume
N	the normal force in a structural element
M_b	the bending moment about y-axis
M_s	the shear force acting along the z-axis
Q	the torsional moment
a	the plate's length

b	the plate’s width
h	the plate’s overall thickness
$\bar{U}$	the axial displacement
q	the transverse bending load

Greek symbols

v	the Poisson's ratio
$\bar{w}$	the transverse displacements
σ	the normal stress
τ	the shear stress

Subscripts

A	steel
T	tungsten inclusions
tot	the total value
b	bending
s	shear